Promotion of $Ni/MgAl_2O_4$ Catalysts with Rare Earths for the Ethanol Steam Reforming Reaction

Agustín E. Galetti, Mariana N. Barroso, Manuel F. Gomez, Luis A. Arrua, Antonio Monzón & M. Cristina Abello

Catalysis Letters

ISSN 1011-372X
Volume 142
Number 12

Catal Lett (2012) 142:1461-1469
DOI 10.1007/s10562-012-0927-9

Springer

Catal Lett (2012) 142:1461–1469
DOI 10.1007/s10562-012-0927-9

Promotion of $Ni/MgAl_2O_4$ Catalysts with Rare Earths for the Ethanol Steam Reforming Reaction

Agustín E. Galetti · Mariana N. Barroso · Manuel F. Gomez · Luis A. Arrua · Antonio Monzón · M. Cristina Abello

Received: 3 July 2012 / Accepted: 10 October 2012 / Published online: 27 October 2012

Abstract Hydrogen production by ethanol steam reforming was studied using Ni catalysts supported over $MgAl_2O_4$ doped with Ce or Pr. $Ni/MgAl_2O_4$–CeO_2 catalyst obtained from nickel nitrate impregnation was selected as the best one (final steady conversion = 95.8 %, carbon formation = 0.4 wt% and activity decay = 6.6 %) under the experimental conditions used in this work.

Keywords Hydrogen · Ethanol steam reforming · Ni catalysts · Carbon deposition

1 Introduction

In recent years, the scientific community has oriented numerous research works for searching new energy sources as a consequence of the limited fossil resources and environmental constraints. In this sense, the use of ethanol from biomass to produce hydrogen has a great potential not only due to its renewable origin but also for its rich hydrogen content. Thus, for the ethanol steam reforming (ESR) reaction, $C_2H_5OH + 3H_2O \rightarrow 6H_2 + 2CO_2$, a maximum yield of 6 mol of hydrogen for each mol of ethanol could be obtained.

Ni supported catalysts have shown to be active and selective in the ethanol steam reforming for producing hydrogen [1–5]. The high C–C bond breaking activity and the relatively low cost compared to noble metals, makes Ni a suitable active phase for this reaction. The main problem for most of these catalysts is the high deactivation rate related to both the formation of carbonaceous deposits and the sintering of metallic nanoparticles. The deactivation by fouling occurs by the covering of the active Ni nanoparticles with graphitic carbon layers formed during the reaction. Simultaneously the formation of carbon nanofibers (CNFs) or even nanotubes (CNTs) can be also observed, but these carbonaceous materials do not deactivate the catalyst [6, 7]. Previous works have shown that the addition of Ce [8] or Pr [9] to Ni-based catalysts increases the resistance to the formation of carbonaceous deposits. Several authors [10, 11] have also agreed that the CeO_2 promotes the removal of carbonaceous species due to the high O_2 storage capacity delivering it to the surface by a redox mechanism. A similar effect was found for PrO_2 [12].

The Ni particle size distribution and the metallic dispersion are also very important factors affecting the carbon deposition mechanism [13, 14] and the rate of carbon formation. It is well known that highly dispersed tiny particles avoid the carbon deposition [15]. The anchorage of Ni particles on the support is affected by the Ni precursor used, the activation pretreatment and the support composition [16, 17].

In addition, suitable supports should be resistant to the high temperatures attained during the ethanol steam reforming, and they also should be able to maintain the metallic dispersion as high as possible during reaction.

A. E. Galetti (✉) · M. N. Barroso · M. F. Gomez · L. A. Arrua · M. C. Abello
Instituto de Investigaciones en Tecnología Química (UNSL-CONICET), Chacabuco y Pedernera, 5700 San Luis, Argentina
e-mail: agugaletti@yahoo.com.ar

M. C. Abello
e-mail: cabello@unsl.edu.ar

A. Monzón
Department of Chemical and Environmental Engineering, Faculty of Science, University of Zaragoza, 50009 Saragossa, Spain

Spinel-like oxides (AB_2O_4) have been proposed as catalytic supports due to the low acidity and resistance to coking and sintering [18, 19]. Thus, Guo et al. [20] have claimed that the use of Ni/$MgAl_2O_4$ during the dry reforming of methane allows to attain higher activity and better stability that using Ni/γ-Al_2O_3. Auprêtre et al. [21] have also obtained an improved deactivation resistance using catalysts supported over $MgAl_2O_4$. Furthermore, in a previous work, we found that $MgAl_2O_4$ was a better support than $ZnAl_2O_4$ [22] due to higher metal–support interaction and higher basicity of Mg–Al oxide spinel, avoiding the coke deposition.

In this work the influence of rare earths (Ce or Pr) addition and the role of Ni precursor on the activity, the resistance to coke and the stability of a series of Ni–Mg–Al catalysts during ethanol steam reforming are studied. The catalysts were prepared by wet impregnation of $MgAl_2O_4$ and characterized by N_2 physisorption, X-ray diffraction, temperature programmed reduction, thermogravimetry analysis under an oxidative atmosphere, Raman spectroscopy and transmission electron microscopy.

2 Experimental

2.1 Catalyst Preparation

Ni catalysts supported on $MgAl_2O_4$ modified with rare earths (Ce or Pr) were prepared. $MgAl_2O_4$ support (MA) was prepared by the citrate method. Citric acid was added to an aqueous solution that contained the stoichiometric quantities of $Al(NO_3)_3{\cdot}9H_2O$ and $Mg(NO_3)_2{\cdot}6H_2O$. An equivalent of acid per total equivalent of metals was used. The solution was stirred for 10 min and held at boiling temperature for 30 min. Then, the solution was concentrated by evaporation under vacuum in a rotavapor at 75 °C until a viscous liquid was obtained. Finally, dehydration was completed by drying the sample in a vacuum oven at 100 °C for 16 h. The sample was calcined in a 100 mL min^{-1} flow under the following program: at 500 °C in N_2 flow for 2 h and then at 700 °C in air for 4 h to remove the carbonaceous residues from citrate chains.

The MA support modified by the addition of 5 wt% of rare earth was prepared by wet impregnation using an aqueous solution of $Pr(CH_3COO)_3{\cdot}xH_2O$ (Aldrich, 99.9 %) or $Ce(CH_3COO)_3{\cdot}xH_2O$. The solvent was evaporated in a rotavapor at 75 °C under vacuum. The samples were dried at 100 °C and calcined in air at 600 °C for 2 h. The modified support was denoted as MAX being X = P from Pr or C from Ce, respectively.

Four supported catalysts with 8 wt% Ni were prepared by the wet impregnation technique using an aqueous solution of $Ni(NO_3)_2{\cdot}6H_2O$ (Nt), or $Ni(CH_3COO)_2{\cdot}4H_2O$ (Ac). The impregnation with acetate was rather difficult due to its very low solubility. After impregnation, the samples were dried and calcined in a 5 % H_2/N_2 flow (200 mL min^{-1}) from room temperature to 600 °C at 10 °C min^{-1} and after they were kept at 600 °C for 2 h. The catalysts were denoted as MAX-Y being X: P or C indicative of rare earth and Y: Ac or Nt indicative of Ni precursor. Hence, MAC-Nt indicates a catalyst with 8 wt% of Ni prepared from nickel nitrate over MAC support.

2.2 Catalyst Characterization

All samples were characterized using different physicochemical methods.

2.2.1 Chemical Composition

Praseodymium, cerium and nickel chemical composition was performed by inductively coupled plasma-atomic emission spectroscopy (ICP) by using a sequential ICP spectrometer Baird ICP 2070 (BEDFORD, USA) with a Czerny Turner monochromator (1 m optical path). Alkali fusion with $KHSO_4$ and a subsequent dissolution with HCl solution brought the samples into solution.

2.2.2 BET Surface Area

BET surface areas were measured by using a Micromeritics Gemini V analyzer by adsorption of nitrogen at −196 °C on 100 mg of sample previously degassed at 250 °C for 16 h under flowing N_2.

2.2.3 X-Ray Diffraction (XRD)

Diffraction patterns were obtained with a RIGAKU diffractometer operated at 30 kV and 20 mA by using Ni-filtered Cu Kα radiation ($\lambda = 0.15418$ nm) at a rate of 3° min^{-1} from $2\theta = 20°$ to 80°. The powdered samples were analyzed without a previous treatment after deposition on a quartz sample holder. The identification of crystalline phases was made by matching with the JCPDS files.

2.2.4 Thermal Gravimetry (TG)

The analyses were recorded using DTG-60 Shimadzu equipment. The samples, ca. 15 mg, were placed in a Pt cell and heated from room temperature to 800 °C at a heating rate of 10 °C min^{-1} with a gas feed (air) of 50 mL min^{-1}. Carbon deposited during reaction on used catalysts was evaluated as.

$$\%C = \frac{w_{coke}}{w_{catalyst}} \times 100$$

where w_{coke} is the coke mass deposited on the catalyst, calculated from the weight loss measured by TGA and $w_{catalyst}$ is the catalyst weight free of carbon remaining after the TG analysis.

2.2.5 Temperature Programmed Reduction (TPR)

Studies were performed in a conventional TPR equipment. This apparatus consists of a gas handling system with mass flow controllers (Matheson), a tubular reactor, a linear temperature programmer (Omega, model CN 2010), a PC for data retrieval, a furnace and various cold traps. The samples were pretreated in a 30 mL min^{-1} flow in He at 300 °C for 30 min before each reduction run. After that, the system was cooled to 25 °C. The samples were subsequently contacted with a 30 mL min^{-1} flow of 5 vol% H_2 in N_2, heated at a rate of 10 °C min^{-1}, from 25 °C to a final temperature of 700 °C and held at 700 °C for 1 h. Hydrogen consumption was monitored by a thermal conductivity detector after removing the formed water. The peak areas were calibrated with H_2(5 vol%)/N_2 mixture injections.

2.2.6 Raman Spectroscopy

The Raman spectra were recorded using a Lab Ram spectrometer (Jobin–Yvon) coupled to an Olympus confocal microscope (100× objective lens were used for simultaneous illumination and collection) and equipped with a CCD with the detector cooled to about −70 °C using the Peltier effect. The excitation wavelength was in all the cases 532 nm (Spectra Physics argon-ion laser). The laser power was set at 30 mW. Integration times ranged from a few seconds to a few minutes depending on the sample. A scanning range between 100 and 2,000 cm^{-1} was applied.

2.2.7 Transmission Electron Microscopy (TEM)

TEM micrographs images were recorded in a FEI Tecnai T20 equipment operated at 200 kV to that the irradiation damages were minimized. Specimens were prepared by standard techniques.

2.3 Catalytic Test

The ethanol steam reforming reaction was carried out in a stainless steel tubular reactor with an internal diameter of 4 mm operated at atmospheric pressure. The reactor was placed in a vertical furnace with control of temperature. The reaction temperature was measured with a coaxial K thermocouple placed inside the sample. The feed to the reactor was a gas mixture of ethanol, water and helium (99.999 % research grade). The liquid mixture of ethanol–water was fed at 0.15 mL min^{-1} to an evaporator (operated at 130 °C) through an isocratic pump. The flow rates of gas stream were controlled by mass flowmeters. The experimental set-up has a low pressure proportional relief valve for early detection of catalytic bed plugging. The molar ratio in the feed was H_2O:C_2H_5OH = 4.9:1 being the ethanol flow 1.02×10^{-3} mol min^{-1}. The molar ratio was near to the optimum one suggested from a study of the energy integration and the maximum efficiency in an ethanol processor for hydrogen production and a fuel cell [23, 24]. The catalyst weight was 50 mg (0.3–0.4 mm particle size range) without any diluent in order to observe possible catalyst deactivation in a short time-frame. The catalyst was heated to reaction temperature under He flow, then the mixture with $C_2H_5OH + H_2O$ was allowed to enter into the reactor to carry out the catalytic test. Fresh samples were used in all the experiments. The reactants and reaction products were analyzed on-line by gas chromatography. H_2, CH_4, CO_2 and H_2O were separated by a 1.8 m Carbosphere (80–100 mesh) column and analyzed by TC detector. Nitrogen was used as an internal standard. Besides, CO was analyzed by a flame ionization detector after passing through a methanizer. Higher hydrocarbons and oxygenated products (C_2H_4O, $C_2H_4 + C_2H_6$, C_3H_6O, C_2H_5OH, etc.) were separated in Rt–U PLOT capillary column and analyzed with FID using N_2 as carrier gas. The homogeneous contribution was tested with the empty reactor. These runs showed an ethanol conversion lower than 5 % at 650 °C.

Ethanol conversion (X_{EtOH}), selectivity to carbon products (S_i), hydrogen selectivity (S_{H_2}) and % conversion loss (%XL) were defined as follows

$$X_{EtOH} = \frac{F_{EtOH}^{in} - F_{EtOH}^{out}}{F_{EtOH}^{in}} \times 100$$

$$S_i = \frac{v_i F_i^{out}}{2\left(F_{EtOH}^{in} - F_{EtOH}^{out}\right)} \times 100$$

$$S_{H_2} = \frac{F_{H_2}^{out}}{3\left(F_{EtOH}^{in} - F_{EtOH}^{out}\right) + \left(F_{H_2O}^{in} - F_{H_2O}^{out}\right)} \times 100$$

$$\%XL = \frac{X_{EtOH}^{0} - X_{EtOH}^{SS}}{X_{EtOH}^{0}} \times 100$$

F_i^{in} and F_i^{out} are the molar flow rates of product "i" at the inlet and outlet of the reactor, respectively, and v_i is the number of carbon atoms in "i". X_{EtOH}^{0} and X_{EtOH}^{SS} are the initial and final steady state ethanol conversions.

3 Results and Discussion

3.1 Catalytic Performance

The overall performance of the catalysts studied during ethanol steam reforming is evaluated in terms of ethanol conversion, product distribution and stability. The evolution of ethanol conversion along the time on stream, at 650 °C, is shown in Fig. 1. A high initial ethanol conversion was observed for all the catalysts. The main products obtained were H_2, CO_2 and CO. Minor amounts of C_2H_4O and CH_4 were also produced. A significant conversion decay was observed for the MAP-Nt catalyst after 150 min of operation attaining a conversion of 68.7 % at 350 min. In fact, this experimental run was interrupted at this time due to the severe increase of the reactor pressure bed. Comparing all the catalysts studied, the final steady state ethanol conversion follows the sequence: MAC-Ac ($X^{SS}_{EtOH} = 97.1$ %) ≅ MAC-Nt ($X^{SS}_{EtOH} = 95.8$ %) > MAP-At ($X^{SS}_{EtOH} = 89.2$ %) > MAP-Nt ($X^{350\ Min}_{EtOH} = 68.7$ %). Consequently, the % conversion loss follows the inverse order: MAP-Nt (31.1 %) > MAP-Ac (14.7 %) > MAC-Nt (6.6 %) > MAC-Ac (2.2 %). Therefore, a lower deactivation is observed with the Ce modified catalysts.

The product distributions over the two MAC samples were very similar. Thus, the hydrogen selectivity was around 74 % and the CO/CO_2 molar ratios were 0.57 and 0.54 for MAC-Nt and MAC-Ac, respectively. For MAP-Ac, the decrease in conversion was accompanied by a decrease in H_2 and CO_2 selectivities and by an increase in C_2H_4O selectivity. Thus, after 350 min of reaction, the hydrogen selectivity was 64.2 %, and the CO/CO_2 molar ratio was 0.75. For MAP-Nt changes in selectivities to H_2, CO and C_2H_4O began at 150 min. At the steady state, the selectivities to acetaldehyde were lower in Ce doped catalysts ($S_{C_2H_4O} = 2.9$ and 5.1 % for MAC-Ac and MAC-Nt, respectively) than Pr doped catalysts ($S_{C_2H_4O} = 9.5$ and 11.0 % for MAP-Ac and MAP-Nt, respectively).

Romero et al. [17]. have attained an ethanol conversion of 87 % with an H_2 selectivity of 68 % and a CO/CO_2 molar ratio equal to 0.72 using a Ni–Mg–Al layered double hydroxide catalyst in steam reforming of ethanol (the reaction time was not reported). These values are near to those obtained over MAC-Y samples. However, the authors claimed no carbon formation which is markedly different from the present work. The substantially less severe operating conditions used by Romero et al. (reaction temperature: 550 °C, inlet ethanol molar fraction: 1 %,

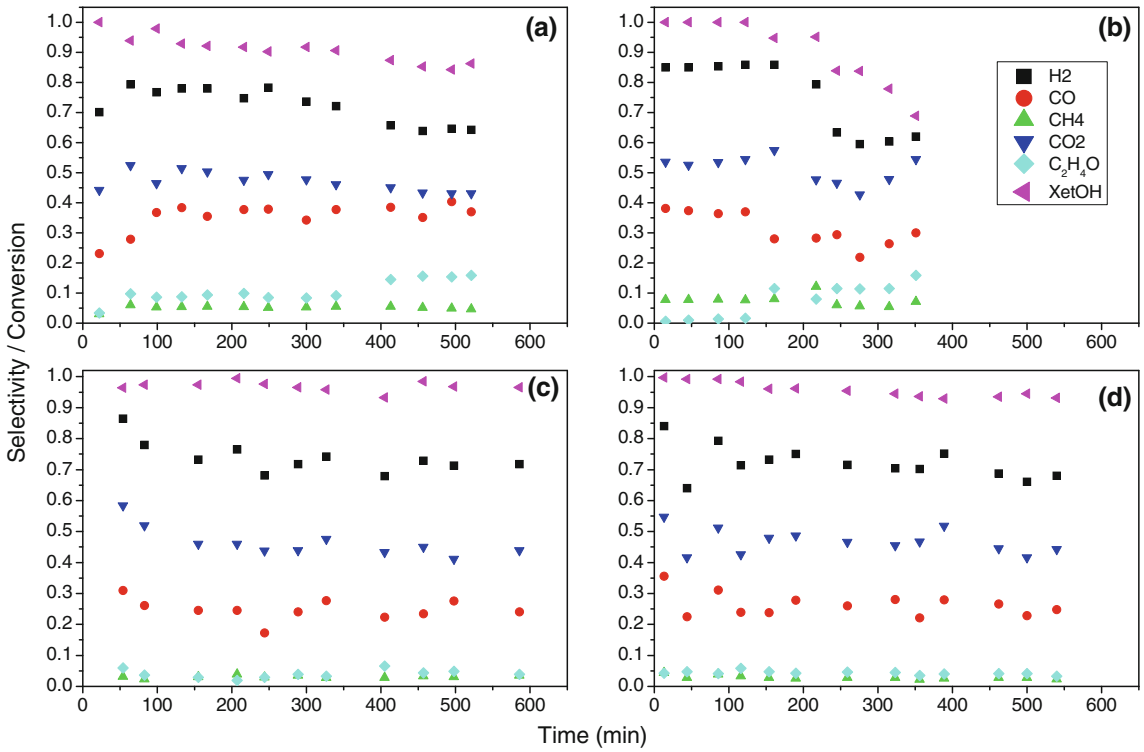

Fig. 1 Product distribution and ethanol conversion in ethanol steam reforming over **a** MAP-Ac; **b** MAP-Nt; **c** MAC-Ac and **d** MAC-Nt catalysts. (*black square*) H_2; (*red circle*) CO; (*green up-pointing triangle*) CH_4; (*blue down-pointing triangle*) CO_2; (*blue diamond*) C_2H_4O; ethanol conversion (*pink left-pointing pointer*)

inert carrier flow: 350 mL min^{-1} and a catalyst:solid inert ratio = 1:10) could explain the different behavior of catalysts.

In a previous work [9], a Ni catalyst supported on $MgAl_2O_4$ (similar to MAP-Ac) but calcined under oxidative atmosphere and with a different impregnation sequence was investigated. It showed a lower ethanol conversion (X_{EtOH} = 80 %), a conversion loss about 20 %, a low carbon deposition and a higher CO formation. Therefore, the results obtained in the present work indicate that the catalysts calcined under a reductive atmosphere and doped with Pr showed an improved catalytic performance increasing the activity, stability and selectivity. Similar results were found for Ni/$ZnAl_2O_4$–CeO_2 catalysts [16]. They showed better performances in ethanol steam reforming when they were calcined under a reductive atmosphere.

3.2 Characterization Results

Results of characterization of the fresh samples and of the support are presented in Table 1. The specific surface area, S_{BET}, of bare support MA was 60 m^2 g^{-1}. In all the cases the BET areas of catalysts were similar ranging between 29 and 36 m^2 g^{-1} and they were not affected by the Ni precursor used. The chemical composition, determined by ICP, indicates that Ni and Ce contents were near the nominal values. However, significant differences in the Pr content with respect to the nominal value were observed probably due to the Pr source was highly hygroscopic [9].

The X-ray diffraction patterns of fresh samples shown in Fig. 2 reveal the reflection lines of $MgAl_2O_4$ (2θ = 31.3°, 36.8°, 44,8°, 55.6°, 59.4° and 65.2°, JCPDS-21-1152) coming from the MA support. The peaks assigned to CeO_2 (2θ = 28.5°, 47.5°, 56.3°, JCPDS 30-0394) are clearly observed in MAC samples, However, weak reflections at 2θ = 28°, 47° and 56° are detected in MAP samples in agreement with the low Pr loadings determined by ICP. They could be assigned to PrO_2 (2θ = 28.7°, 33.2°, 47.7°, 56.6°, JCPDS-24-1006) or Pr_6O_{11} considered as an oxygen-deficient modification of PrO_2 (2θ = 28.2°, 47°, 32.7°, 55.7°, JCPDS-42-1121). In all the samples peaks assigned to Ni^0 (2θ = 44.5°, 51.8°, JCPDS 4-0850) are detected due to the reductive atmosphere of calcination treatment. The presence of the Ni^0 diffraction peaks indicates that an important part of Nickel is present as metallic aggregates after pasivation by the exposure to the air. The crystallite particle size was estimated by the Scherrer equation for the second most intense peak at 2θ = 51.8° corresponding to (200) plane of Ni^0, due to the proximity of the most intense peak at 2θ = 44.5°, corresponding to (111) plane, with that at 44.8° belonging to the $MgAl_2O_4$. These values, d^f_{Ni}, are shown in Table 1. By XRD, the samples prepared from nickel acetate showed higher particle sizes than those from nitrate salt. However, TEM observations of fresh samples (images not shown) indicate the presence of small particles well distributed over the support. Wang and Lu [25] have reported the effect of nickel precursor on catalytic behavior of Ni/Al_2O_3 catalysts in CO_2 reforming of methane. They have found that the interaction between nickel oxide and support was dependent on the precursor used and this affected the nickel dispersion. Thus, the particle size of Ni prepared by nitrate salt was significantly smaller than that of catalysts prepared from nickel chloride and nickel acetylacetonate.

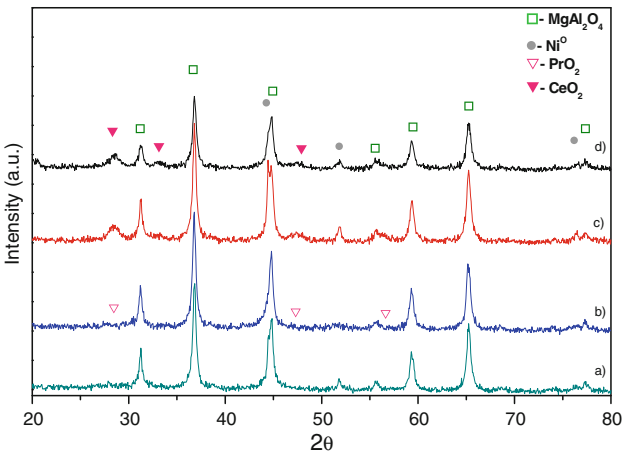

Fig. 2 Diffraction patterns of fresh samples. **a** MAP-Ac; **b** MAP-Nt; **c** MAC-Ac; **d** MAC-Nt

Table 1 Characteristics of fresh catalysts

Sample	Chemical composition (wt%)		d^f_{Ni} (nm)[b]	S_{BET} (m^2 g^{-1})
	Ni	RE[a]		
MA	–	–	–	60
MAP-Ac	6.8	2.6	42	29
MAP-Nt	8.6	2.9	–	30
MAC-Ac	7.0	6.5	28	36
MAC-Nt	8.1	5.9	16	32

Nominal loading: 8.0 wt% Ni and 5.0 wt% RE

[a] Rare earth (Pr or Ce)

[b] Calculations are based on (200) diffraction lines for Ni^0

The TPR profiles of fresh catalysts are illustrated in Fig. 3. In spite of the calcination in reductive atmosphere and the presence of Ni^0 (as shown by XRD), in all the cases a noticeable hydrogen consumption was observed. Peaks centered at 323 and 291 °C were observed for MAP and MAC samples, respectively. These values are in agreement with the temperatures of maximum weight loss in TG experiments of precursors under reductive atmosphere (not shown): 318 and 279 °C for MAP and MAC catalysts, respectively. This hydrogen consumption of MAX samples

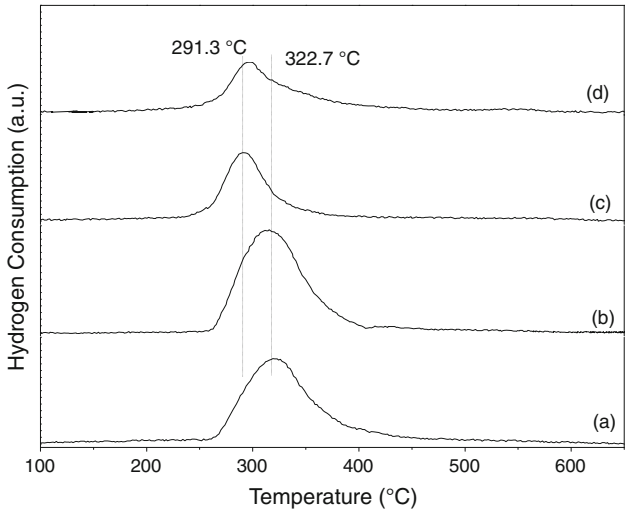

Fig. 3 Temperature programmed reduction profiles for fresh catalysts. **a** MAP-Ac; **b** MAP-Nt; **c** MAC-Ac; **d** MAC-Nt

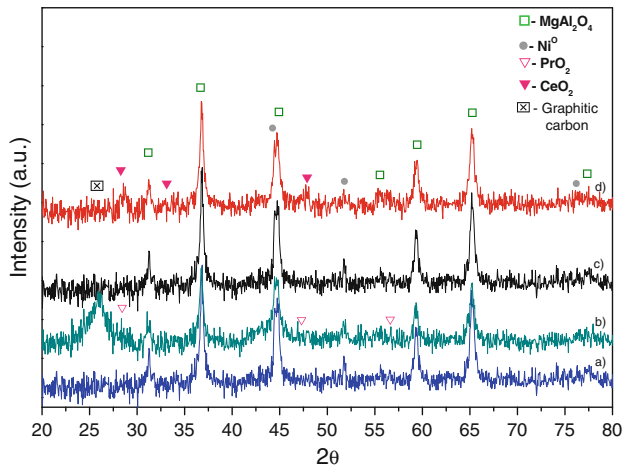

Fig. 4 Diffraction patterns of samples used in ethanol steam reforming. **a** MAP-Ac; **b** MAP-Nt; **c** MAC-Ac; **d** MAC-Nt

Table 2 Characteristics of catalysts after being used in ethanol steam reforming reaction

Sample	[a]d^{u}_{Ni}			
	nm	%XL	%C	I_D/I_G
MA	–	–	–	–
MAP-Ac	41	14.7	1.0	1.03
MAP-Nt	24	31.1	134.2	1.26
MAC-Ac	33	2.2	24.1	1.42
MAC-Nt	–	6.6	0.4	1.22

[a] Calculations are based on (200) diffraction line for Ni^0

could be attributed to: (i) the reduction of Ni^{2+} small particles which kept unreduced after the calcination step in reductive atmosphere; (ii) the reduction of Ni^{2+} species

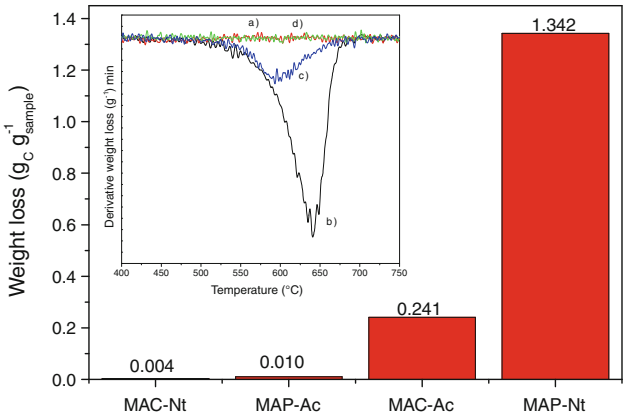

Fig. 5 Weight loss and its derivative (inserted) for catalysts used in ethanol steam reforming. **a** MAP-Ac; **b** MAP-Nt; **c** MAC-Ac; **d** MAC-Nt

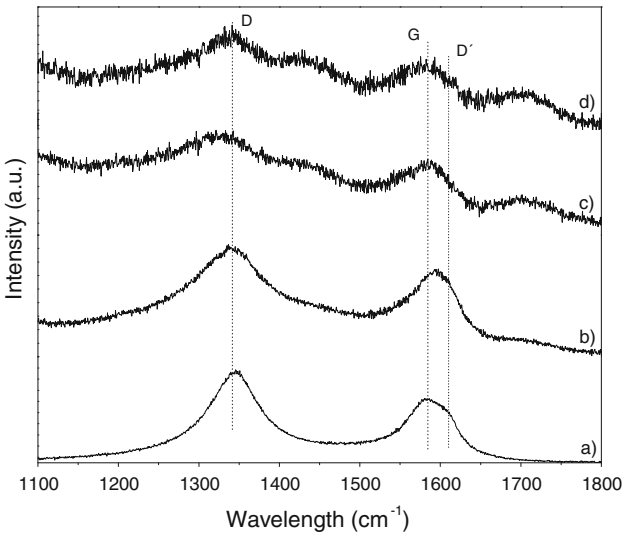

Fig. 6 Raman spectra of catalysts used in ethanol steam reforming. **a** MAP-Ac; **b** MAP-Nt; **c** MAC-Ac; **d** MAC-Nt

oxidized by oxygen after the air exposure, and (iii) eventually to the surface reduction of dopant oxides ($Pr^{4+} \rightarrow Pr^{3+}$; $Ce^{4+} \rightarrow Ce^{3+}$). To examine the two first assumptions a TPR experiment carried out over in situ pretreated MAC precursor sample under reductive atmosphere led to a negligible hydrogen consumption. Therefore, during the calcination procedure Ni^{2+} species were almost quantitatively reduced to Ni^0. After that TPR experiment the sample was cooled down in the reductive mixture at room temperature and then an oxygen flow was allowed to enter to the reactor. Afterwards, a new TPR experiment was carried out and an important hydrogen consumption was observed which could be atributted to the reduction of Ni^{2+} oxidized by air at room temperature. The H_2 uptakes on MAP samples were higher than those on MAC samples. The surface RE oxides could also be oxidized after air

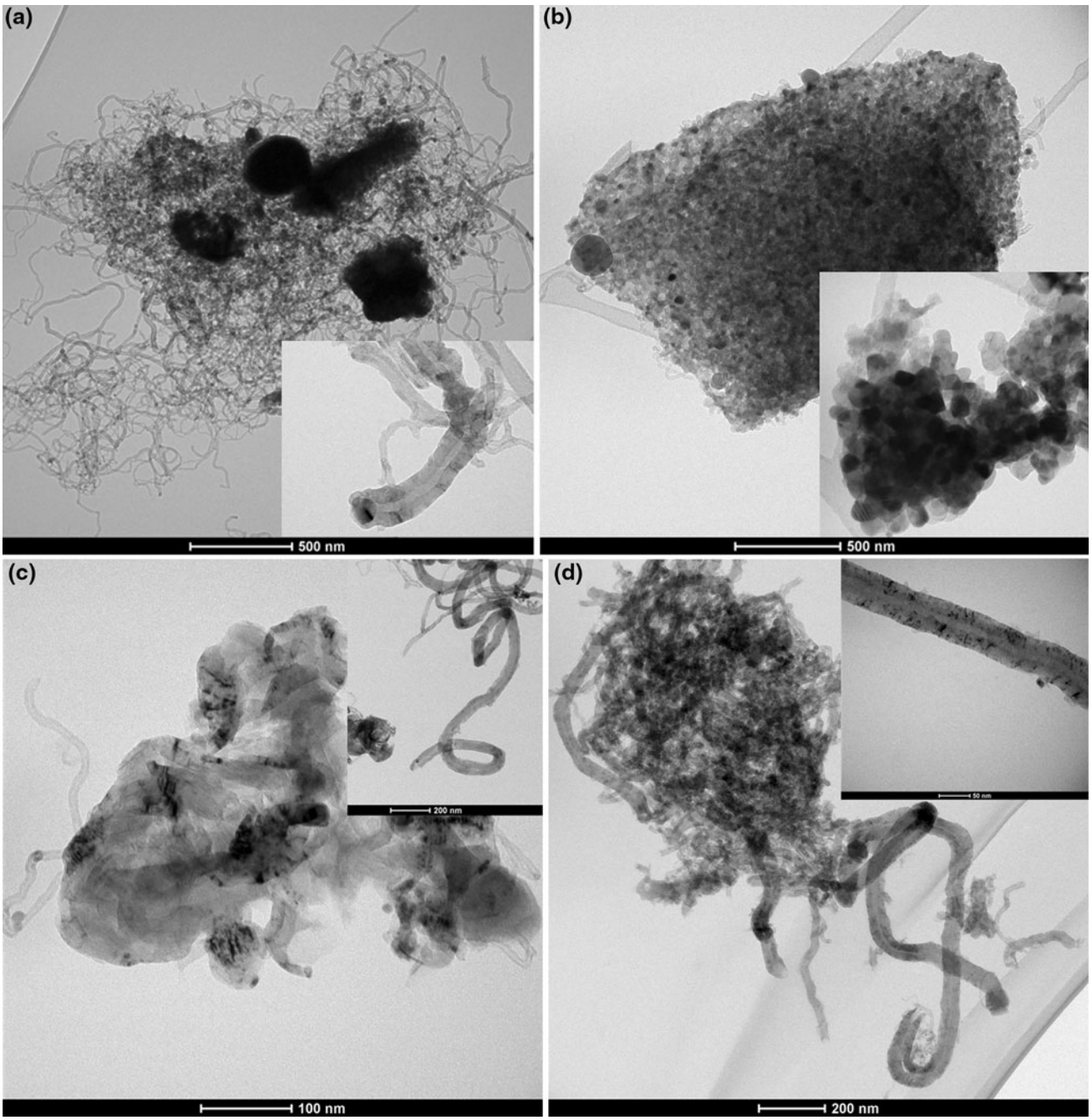

Fig. 7 TEM micrographs of catalysts after ESR at 650 °C. **a** MAC-Ac; **b** MAC-Nt; **c** MAP-Ac: **d** MAP-Nt

exposure. Tarditti et al. [26] have shown by XPS that Ce^{3+}/Ce^{4+} and Pr^{3+} are present at the catalytic surface after H_2 reduction. Then the contribution by reoxidation could be higher over the Pr catalysts and this should explain the higher H_2 consumption in the TPR experiments. The reduction of the oxidized particles occurs at a temperature subtantially lower than the reaction temperature.

XRD patterns of samples after reaction are presented in Fig. 4. The particle sizes, d^{u}_{Ni}, are also shown in Table 2. These values suggest a higher degree of sinterization on MAP-Nt sample which was the catalyst with the higher decay of conversion. In the diffraction pattern of MAP-Nt sample the reflection line (002) corresponding to graphitic carbon is clearly observed ($2\theta = 26.4°$, JCPDS 41-1487) and its intensity is in agreement with the carbon amount detected by TG-TPO (further shown).

The carbon amounts for used samples quantified by TG-TPO are shown in Fig. 5. There are marked differences in the carbon amounts deposited over the catalysts during the reaction, being the order MAP-Nt > MAC-Ac ≫ >

MAP-Ac > MAC-Nt. Two oxidation zones could be detected (insert Fig. 5). For MAC-Ac the more important weight loss is around 596 °C whereas for MAP-Nt is at 642 °C. These facts could indicate the presence of two different kinds of carbonaceous deposits with different graphitization extent.

The nature and characteristics of these deposits are also studied by Raman spectroscopy. In Fig. 6, the Raman spectra of used samples are shown in the range of 1,100–1,800 cm^{-1}. In all the cases, two broad bands centered at 1,579 cm^{-1} (G band) and 1,344 cm^{-1} (D band) are observed, this has been extensively studied in literature. They are attributed to the stretching mode of carbon sp^2 bonds of the typical graphite and to the vibrations of carbon atoms with dangling bonds in disordered graphite planes, respectively. Besides, the band at 1,609 cm^{-1} known as D′ band [27, 28] can not be ruled out. This band is usually associated with defects which break the translational symmetry of the graphene sheet [29]. In Table 2 the I_D/I_G intensity ratios are shown. The values follow the order of MAC-Ac > MAP-Nt ≅ MAC-Nt > MAP-Ac. A higher amount of ordered structures could be inferred on MAP-Ac sample whereas the lower amount of them were found on MAC-Ac.

Representative TEM micrographs of catalysts after 10 h of time on stream are shown in Fig. 7. Most part of the carbonaceous deposits are carbon fibres and nanotubes. Despite the analogous structure of carbon deposits, it is evident that a lower amount of filaments is observed on MAC-Nt and MAP-Ac in agreement with TG-TPO results. The micrograph for the used MAC-Ac catalyst, Fig. 7a, shows an important amount of hollow carbon nanofibers bearing at the tip Ni particles having a size roughly equal to that of the internal diameter of carbon nanofibers. However, the micrograph for used MAC-Nt, Fig. 7b, reports a lower amount of carbon and free of carbon nanofibers regions.

The post reaction characterization does not reveal a clear correlation among conversion loss, carbon amounts and catalyst nature. The lowest conversion loss (%XL = 2.2) corresponds to MAC-Ac sample. However, the amount of carbon nanofibers, around 24 %, is significant. The high carbon amount and the low conversion loss is a strong indication that metal particles remain mainly uncovered, as observed by TEM, thus resulting in much lower deactivation rates than those expected by encapsulating carbon. This MAC-Ac sample shows a very good stability, Fig. 2, but the high carbon deposition observed will affect the long-term stability of the catalyst and will cause fail to the reactor operation. On the other hand, the MAC-Nt catalyst presents a %XL = 6.6, a low carbon amount deposited after 10 h of time on stream (0.4 %) and a substantially lower amount of CNFs. For MAP-Nt and MAP-Ac catalysts the conversion losses are higher, 31.3 and 14.7 %, respectively. MAP-Nt catalyst is initially very active but it forms significant amounts of carbon nanofibers and also suffers sintering. In summary, the experimental results indicate that there is not a clear relationship between the carbon content and the degree of deactivation.

The catalysts supported on $MgAl_2O_4$ modified by Ce demonstrate a good performance during ethanol steam reforming at mild operating conditions. However, long term stability tests and regeneration studies become necessary. In comparison with similar catalysts supported over $ZnAl_2O_4$ [16], the Mg spinel is a better support due to changes in its acid- base properties and the strongest metal–support interaction.

4 Conclusions

Four Ni catalysts supported on $MgAl_2O_4$ modified by Pr or Ce addition were prepared by impregnation. Two nickel sources were used: nickel nitrate and nickel acetate. The catalyst prepared from nickel nitrate and dopped with Pr showed the lowest average Ni particle size and it was very active during the first 150 min in reaction. After 350 min, the ethanol conversion markedly decreased and a significant amount of carbon is formed causing the blocking of the reactor. Therefore, a small Ni^0 particle size did not guarantee a higher resistance to carbon deposition but increased the sintering of the Ni particles.

The catalysts modified by Ce were more selective to H_2 and to CO_2. They showed higher catalyst stability than those modified by Pr. The Ni(Ac)/$MgAl_2O_4$–CeO_2 catalytic system showed the highest ethanol conversion at the conditions studied (steady ethanol conversion = 97.1 % and conversion loss = 2.2 %) under mild operating conditions (ethanol concentration = 7.8 %, feed molar ratio H_2O:C_2H_5OH = 4.9, reaction temperature = 650 °C and W/F_{EtOH} = 49 g min mol^{-1}_{EtOH}) but it showed an abundant carbon filament formation. Ni(Nt)/$MgAl_2O_4$–CeO_2 catalyst was also very active (steady etanol conversion = 95.8 %) with a low amount of carbon (0.4 wt%) and a low conversion loss (6.6 %) under the same conditions. The hydrogen selectivity was 74 % and the main gaseous C-products were CO_2 and CO. In summary, this catalyst has the best overall catalytic performance under the experimental conditions used in this work.

Acknowledgments Financial supports are acknowledged to CONICET, ANPCyT and Universidad Nacional de San Luis. The funds from the ANPCyT to buy the Raman instrument are also grateful (PME 87-PAE 36985).

References

1. Biswas P, Kunzru D (2007) Int J Hydrogen Energy 32:969–980
2. Sánchez-Sánchez MC, Navarro RM, Fierro JLG (2007) Int J Hydrogen Energy 32:1462–1471

3. Frusteri F, Freni S, Chiodo V, Spadaro L, Di Blasi O, Bonura G, Cavallaro S (2004) Appl Catal A 270:1–7
4. Liberatori JWC, Ribeiro RU, Zanchet D, Noronha FB, Bueno JMC (2007) Appl Catal A 327:197–204
5. Comas J, Mariño F, Laborde M, Amadeo N (2004) Chem Eng J 98:61–68
6. Latorre N, Cazaña F, Martínez-Hansen V, Royo C, Romeo E, Monzón A (2011) Catal Today 172:143–151
7. Latorre N, Romeo E, Cazaña F, Ubieto T, Royo C, Villacampa JI, Monzón A (2010) J Phys Chem C 114:4773–4782
8. Galetti A, Gomez M, Arrúa L, Cristina Abello M (2008) Appl Catal A 348:94–102
9. Noelia Barroso M, Galetti A, Cristina Abello M (2011) Appl Catal A 394:124–131
10. Trovarelli A (2002) Catalysis by ceria and related materials. Catalytic science series, vol 2. Imperial College Press, London
11. da Silva A, de Souza K, Jacobs G, Graham U, Davis B, Mattos L, Noronha F (2011) Appl Catal B 102:94–109
12. Gallego G, Marin J, Batiot-Dupeyrat C, Barrault J, Mondragón F (2009) Appl Catal A 369:97–103
13. Rostrup-Nielsen J, Trimm DL (1977) J Catal 48:155–165
14. Chen D, Christensen KO, Ochoa-Fernández E, Yu Z, Totdal B, Latorre N, Monzón A, Holmen A (2005) J Catal 229:82–96
15. Chen X, Tadd A, Schwank J (2007) J Catal 251:374–387
16. Galetti A, Gomez M, Arrua L, Cristina Abello M (2011) Appl Catal A 408:78–86
17. Romero A, Jobbagy M, Laborde M, Baronetti G, Amadeo N (2010) Catal Today 149:407–412
18. Sehested J, Gelten JAP, Remediakis IN, Bengaard H, Norskov JK (2004) J Catal 223:432–443
19. Gadalla AM, Bower B (1988) Chem Eng Sci 43:3049–3062
20. Guo J, Lou H, Zhao H, Chai D, Zheng X (2004) Appl Catal A Gen 273:75–82
21. Auprêtre F, Descorme C, Duprez D, Casanave D, Uzio D (2005) J Catal 233:464–477
22. Barroso MN, Gomez MF, Arrua LA, Abello MC (2009) Actas XVI CAC, Buenos Aires
23. Francesconi JA, Mussati MC, Mato RO, Aguirre PA (2007) J Power Sources 167:151–161
24. Perna A (2007) Int J Hydrogen Energy 32:1811–1819
25. Wang S, Lu GQ (1998) Appl Catal A 169:271–280
26. Tarditi A, Barroso MN, Galetti AE, Gomez MF, Arrua LA, Cornaglia L, Abello MC (2012) XXIII Congreso Iberamericano de Catálisis. Santa Fe, Argentina
27. Maldonado S, Morin S, Stevenson KJ (2006) Carbon 44:1429–1437
28. Cornaglia LM, Múnera J, Irusta S, Lombardo EA (2004) Appl Catal A 263:91–101
29. Barros EB, Souza Filho AG, Son H, Dresselhaus MS (2007) Vib Spectrosc 45:122–127